Science of the Total Environment 884 (2023) 163818

Contents lists available at ScienceDirect

Science of the Total Environment

journal homepage: www.elsevier.com/locate/scitotenv

Canopy composition drives variability in urban growing season length more than the heat island effect

Michael Alonzo [a,*], Matthew E. Baker [b], Joshua S. Caplan [c], Avery Williams [a], Andrew J. Elmore [d]

[a] Department of Environmental Science, American University, Washington, DC 20016, USA
[b] Department of Geography & Environmental Systems, University of Maryland, Baltimore County, Baltimore, MD 21250, USA
[c] Department of Architecture and Environmental Design, Temple University, Ambler, PA 19002, USA
[d] Appalachian Laboratory, University of Maryland Center for Environmental Science, Frostburg, MD 21532, USA

HIGHLIGHTS

- Cities offer a phenological preview of natural forest response to global change.
- How much do urban tree planting preferences (e.g., species) influence phenology?
- We employ >400 PlanetScope images to estimate individual tree phenology in a city.
- Species and plant functional type mixtures governed phenology more than heat.

GRAPHICAL ABSTRACT

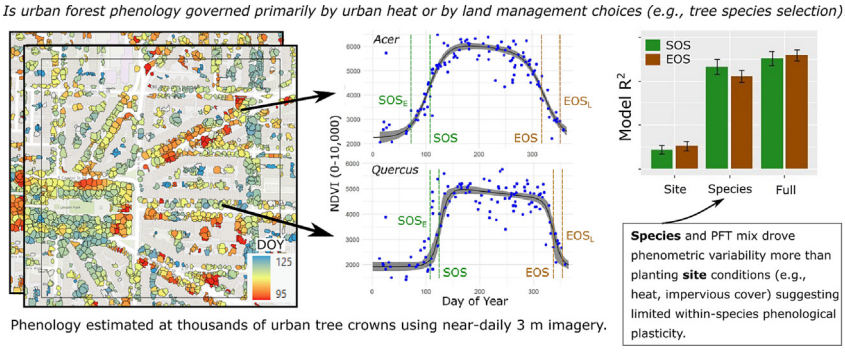

ARTICLE INFO

Editor: Shuqing Zhao

Keywords:
Phenology
High-resolution remote sensing
Urban heat island

ABSTRACT

The elevated heat of urban areas compared to their surroundings makes humid temperate cities a useful preview of future climate effects on natural forest phenology. The utility of this proxy rests on the expectation that trees in urban areas alter their phenology in response to warmer site conditions in spring and fall. However, it is possible that apparent lengthening of the growing season is instead governed by human-driven tree species selection and plant functional type (PFT; trees, shrubs, turfgrass) heterogeneity typical of managed landscapes. Without the use of highly spatially and temporally resolved remote sensing data, the roles of tree taxonomy and local site characteristics (e.g., impervious cover) in controlling phenology remain confounded. To understand the drivers of earlier start of season (SOS) and later end of season (EOS) among urban trees, we estimated individual tree phenology using >130 high-resolution satellite images per year (2018–2020) for ~10,000 species-labeled trees in Washington, DC. We found that species identity alone accounted for 4× more variability in the timing of SOS and EOS compared with a tree's planting location characteristics. Additionally, the urban mix of PFTs may be more responsible for apparent advances in SOS (by between 1.8 ± 1.3 and 3.5 ± 1.3 days) than heat per se. The results of this study caution against associating longer growing seasons in cities—observed in moderate to coarse resolution remote sensing imagery—to within-species phenological plasticity and demonstrate the power of high-resolution satellite data for tracking tree phenology in biodiverse environments.

* Corresponding author.
E-mail address: alonzo@american.edu (M. Alonzo).

http://dx.doi.org/10.1016/j.scitotenv.2023.163818
Received 16 February 2023; Received in revised form 24 April 2023; Accepted 25 April 2023
Available online 29 April 2023

1. Introduction

Leaf phenology influences the fluxes of water and energy between the Earth's surface and the atmosphere as it defines the period when trees are physiologically active. Predicting changes in leaf phenology under global change scenarios is therefore highly valuable for forecasting climate-induced shifts in these fluxes. Cities present an empirical basis for quantifying such effects because many cities are several degrees warmer than their surroundings, meaning that urban trees currently exhibit phenological responses we might expect from non-urban forests several decades in the future. Moreover, understanding environmental and biological controls on tree phenology can help to optimize strategies for climate-ready urban planning. The phenology of urban trees governs the availability of ecosystem services for residents (Zhang and Brack, 2021), alters the surface energy balance (Penuelas et al., 2010), and mediates ecological niche quality for urban fauna (Visser et al., 1998). Those who manage city landscapes therefore must understand the drivers and extents of phenological change in order to manage for tree climate resilience and the continued provisioning of ecosystem services (Núñez-Florez et al., 2019).

In temperate zones, urban trees generally have an earlier start of season (SOS) and a later end of season (EOS) compared to rural surroundings (Li et al., 2017a; Melaas et al., 2016). These phenological shifts have largely been attributed to the urban heat island effect, which arises when a landscape dominated by transpiring vegetation is replaced with impervious surfaces and buildings (Oke, 1982). However, urban areas are extremely heterogeneous at fine spatial scales with respect to site factors (e.g., air temperature, substrate, water availability, shade) as well as the composition of plant communities. Species identities and plant functional types (PFT, e.g., trees, shrubs, turfgrass) can vary widely across urban areas because they are often highly managed, reflecting historical planting and development patterns. Thus, the extent to which urban tree phenology varies might be attributed to site factors, spatial variation in plant composition, or some combination of the two.

In North American broadleaf deciduous forests, satellite-based studies have found urban-rural differences in growing season length (GSL) from 2 to upwards of 22 days. Overall, there has been greater certainty in estimates of SOS compared to EOS, both in terms of timing and isolation of drivers (Jochner and Menzel, 2015). While SOS can be linked to variability in winter and spring temperatures (Jochner and Menzel, 2015; Melaas et al., 2016), urban EOS is more difficult to characterize and is potentially driven by summer or fall air temperatures (Lu and Keenan, 2022), local CO_2 levels (Wang et al., 2019), urban density (D. Li et al., 2022), light pollution, soil conditions, irrigation, or nutrient availability (Wohlfahrt et al., 2020). The influence of planting site on variation in phenological metrics (hereafter "phenometrics") has thus far been examined largely independently of species identity or PFT due to measurement limitations (both remote sensing and ground-based). However, several studies have documented variation in phenometrics within individual species associated with urban site conditions, namely the imperviousness of surroundings and the proximity to urban canyons and water (Chi et al., 2022; Granero-Belinchon et al., 2020).

Plant functional types and tree species identities are typically quite different between managed urban landscapes and surrounding rural or natural landscapes. At a coarse taxonomic grain, urban and peri-urban development choices determine the ratios of land cover types and thus the dominant PFTs. In temperate regions, cultivated trees, shrubs, and turfgrass are interspersed with varying quantities of natural vegetation and impervious surface (Cadenasso et al., 2007). Moreover, the relative cover of turfgrass vs. trees has implications for phenological analyses, as cultivated grass often has earlier SOS and later EOS (Zipper et al., 2016). Understory species, especially invasive or native shrubs, may also have distinct phenological niches, thus influencing phenometrics (Fridley, 2012; Shustack et al., 2009). Tree species composition also varies along urbanization gradients —mediated by the strength of the local climate filter (Jenerette et al., 2016; Swan et al., 2017)—typically with more introduced species present at the urban end of the gradient. Community-level phenological research has been hindered by an inability to monitor all species within that community (Cleland et al., 2007). This is particularly true for remote sensing studies, in which large spatial extents preclude extensive, species-level ground truthing. Yet, there is evidence of that coexisting species can exhibit strong phenological differences and, at the same time, exhibit limited phenological plasticity within species (Cleland et al., 2007; Tang et al., 2016). The former adds noise to coarse to moderate pixel-scale analyses (e.g., those using MODIS or Landsat imagery), obscuring the drivers of change, while the latter implies that individual species may have more limited responses to urban heat than anticipated.

Given the high degree of spatial heterogeneity and the rapid rates of land cover change in urban environments, new methods are necessary for mapping and monitoring ecosystem functions in cities (Zhu et al., 2019). Urban air temperature is now quantifiable citywide at fine spatial resolution, allowing us to determine how local climate is modified by canopy and impervious surface cover (Alonzo et al., 2021; Ziter et al., 2019). Connections between these site conditions and phenology have been elusive due to insufficient satellite resolution and a lack of information on subpixel species composition (Zipper et al., 2016). In this study we present and apply a method for monitoring urban leaf phenology using high-resolution satellite imagery that is practical at regional extents yet implemented at the scale of individual tree crowns. We implemented this method to map all trees within our Washington, DC study area between 2018 and 2020. With this map, of tree-only phenology, we could then evaluate the influence of species and PFT mixing on Landsat and MODIS-scale phenometrics. For a subset of ~10,000 street tree crowns—for which we have field knowledge of species identity for 29 common species—we followed a phylogenetic mixed modeling approach to quantify the contribution of species and site factors to urban tree phenophase timing.

2. Materials and methods

The primary objective of this study was to compare the relative influence of plant functional type and species composition to those of planting site characteristics on tree phenology in an urban setting. Doing this observationally required sampling many tree crowns spanning the range of common tree species across the widest-available gradient of planting conditions (e.g., imperviousness of surroundings). Specifically, we quantified the phenological timing (i.e., the start and end of season, or SOS and EOS, respectively) for individual trees from satellite imagery at high temporal and spatial resolution and covering much of Washington, DC, USA, through three growing seasons (2018–2020; data aggregated). Statistical modeling of tree-level variation in SOS and EOS was undertaken using ordinary least squares regression when species information was not included or phylogenetic generalized least squares (PGLS; Revell, 2010) mixed models when species identities were included. To understand the impact of spatial resolution (and thus spectral mixtures) on these estimates, we compared our crown-scale estimates to those made using either 30 m or 250 m simulated pixels to reflect current, common methods. Finally, given our interest in understanding the importance of species composition in driving urban phenological signals, we sought to quantify species phenometric synchronicity across years by conducting separate analyses on each of our three years of satellite data.

2.1. Study area

The study area encompassed most of Washington, DC, USA (Fig. 1). DC is a humid-subtropical city with a population of approximately 700,000 residents (Beck et al., 2018). It has tree canopy cover of ~38 % and impervious surface cover of ~39 % (Alonzo et al., 2021). The trees are predominantly broadleaved deciduous species, with a small minority being conifers.

2.2. Geospatial data and processing

For each growing season in 2018–2020, we downloaded at least 130, PlanetScope 4-band, top-of-atmosphere radiance images (<10 % cloud

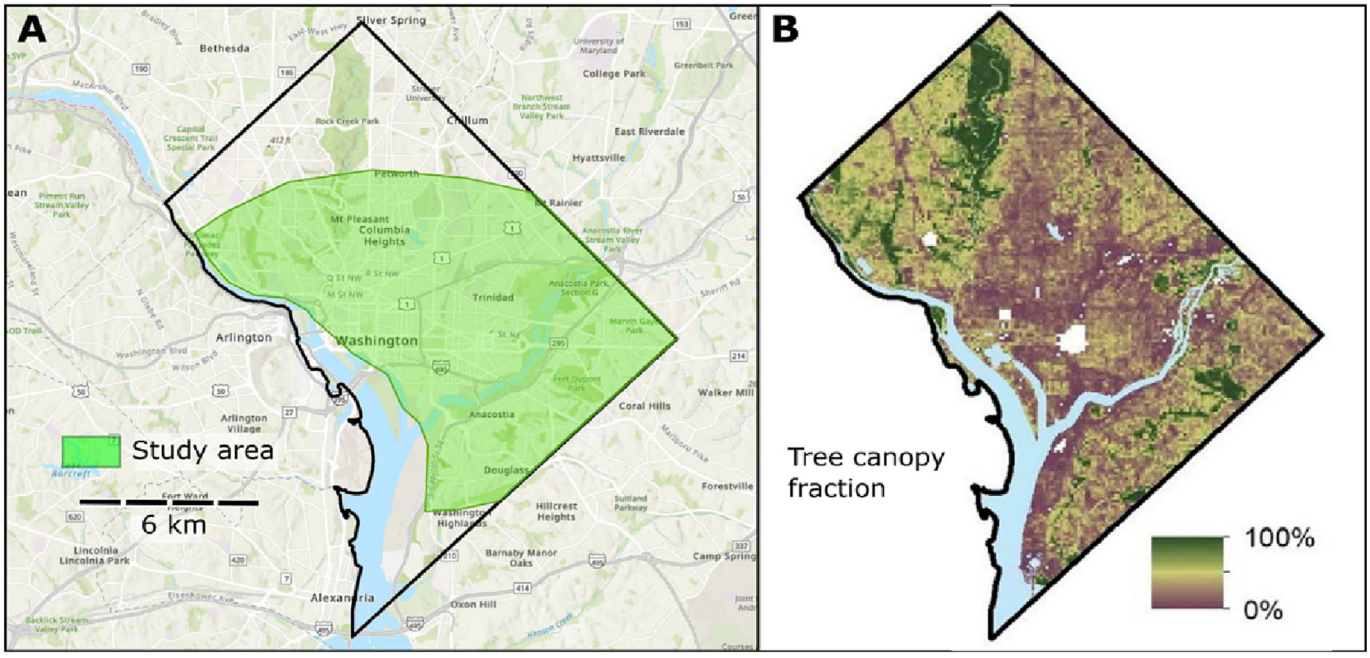

Fig. 1. A) Study area as determined by the minimum number of PlanetScope 4-band images available annually (n = 130). This area contained >63,000 street trees (from 29 important species) with labeled species identities. B) Tree canopy fraction for 100 m pixels in Washington, DC (Alonzo et al., 2021).

cover, <3 degrees off-nadir view angle) with nominal 3 m spatial resolution (Planet, 2021). Images were radiometrically normalized using empirical line correction–with spectrally invariant targets spanning a range of brightness values (e.g., asphalt to white roof)–to a high-quality base image from 2019 (Schott et al., 1988). The normalized difference vegetation index (NDVI; Tucker, 1979) was calculated for each image. To summarize object-scale NDVI, polygons were created for the citywide dataset using the simple linear iterative clustering (SLIC) image segmentation algorithm (Achanta et al., 2012). In addition to crowns, we segmented low vegetation and grass. For street trees, given accurately-geolocated center points, we chose to forgo use of the SLIC segments and instead simply buffered each point by 3 m to create the polygons. The 3 m distance was chosen based on visual assessment, though 2 m buffers were tested and did not lead to appreciably different modeling results. Finally, we extracted the NDVI pixel values within each image object, including the crown polygons as well as n = 2621 randomly distributed "Landsat like", 30 m and n = 320 "MODIS like", 250 m plots. Each image object, for a given date, was ultimately assigned the 75th percentile NDVI pixel value as a means to limit the inclusion of non-vegetation data (Alonzo et al., 2014).

We fit a 7-parameter double logistic function to the 3-year aggregated NDVI time series extracted from each polygon (Fig. 2D; Elmore et al., 2012). Fitting was accomplished using the Levenberg-Marquardt algorithm, implemented via the R code library *nlsLM*. To increase the likelihood of fit convergence, we removed outliers using a smoothing spline fit in the previous step. Two of the final fit parameters capture the day of year (DOY) with the most rapid increase in NDVI in the spring and the most rapid decrease in NDVI in the fall. We define these days as the SOS and EOS phenometrics. We additionally determined the pair of DOYs corresponding to maximum concavity; these represent the initiation of green-up (SOS_E, where E is "early") and the end of leaf senescence (EOS_L, where L is "late"; Fig. 2D). Uncertainty in each phenometric, reported as the 95 % confidence interval, was quantified with bootstrapping (n = 1000 iterations) when fitting the double logistic function (Elmore et al., 2012). This uncertainty largely reflects variability in the fit due to data gaps on cloudy days.

In addition to the above, we fit the double logistic function to NDVI data from each of the three years separately so we could compare our phenological estimates with those from the Multi Source Land Surface Phenology dataset (MS-LSP; Bolton et al., 2020). Annual fits were used to calculate six additional NDVI percentile metrics capturing three stages each of "green-up" (denoted g15, g50, and g90, where numbers indicate percentiles) as well as senescence or "brown-down" (denoted b90, b50, and b15, where numbers again indicate percentiles). These fits were only generated on the subset of 30 m plots with high fractional vegetation cover to facilitate alignment with Harmonized Landsat-Sentinel (HLS) imagery, on which the MS-LSP dataset was based. Given the high correspondence between spline and double logistic fits in this ecosystem, the percentile metrics calculated on the latter fit we assumed to adequately represent those from the former. Nevertheless, we ultimately elected to use the percentile metrics for validation purposes only, as the 7-parameter double logistic fit was better suited for parsing the processes of summer greendown from end of season. We found strong agreement spanning the growing seasons between the annual, PlanetScope-derived metrics and MS-LSP (R^2 = 0.94; Fig. S1). The level of correspondence found in this study is consistent with previous imagery comparison efforts (Cheng et al., 2020; Moon et al., 2021).

Additional geospatial datasets were acquired or created to serve as candidate predictor variables in statistical models of phenometrics (Table 1). We sought to cover the range of spatial variables, of potential interest, that relate to each tree's function in a given planting location. Of course, not all variables can easily be measured at the citywide scale (e.g., soil moisture), which is a limitation of this type of study. A dataset describing species identity and geolocation for 63,019 street trees was obtained from the DC Urban Forestry Department (Table 2). Species were chosen for this study based on the occurrence frequency of street trees within our study area (Fig. 1). There were 29 species with >100 individuals in the study area (Table 2). In many cases, to create predictor variables, we extracted mean pixel values from the relevant raster datasets (e.g., *imperviousness*, *tree_canopy*) within a 90 m buffer around each crown polygon following Alonzo et al. (2021). The *air_temp* variable came from a dataset collected on August 28, 2018, when nine cars measured air temperature throughout the city >70,000 times, which were used to spatially interpolate temperature maps at three times of day (predawn, afternoon, evening; Shandas et al., 2019). Given that these data were collected on a single day, we consider them to be a static depiction of the air temperature anomaly across the study area, making them a useful characterization of the urban heat island.

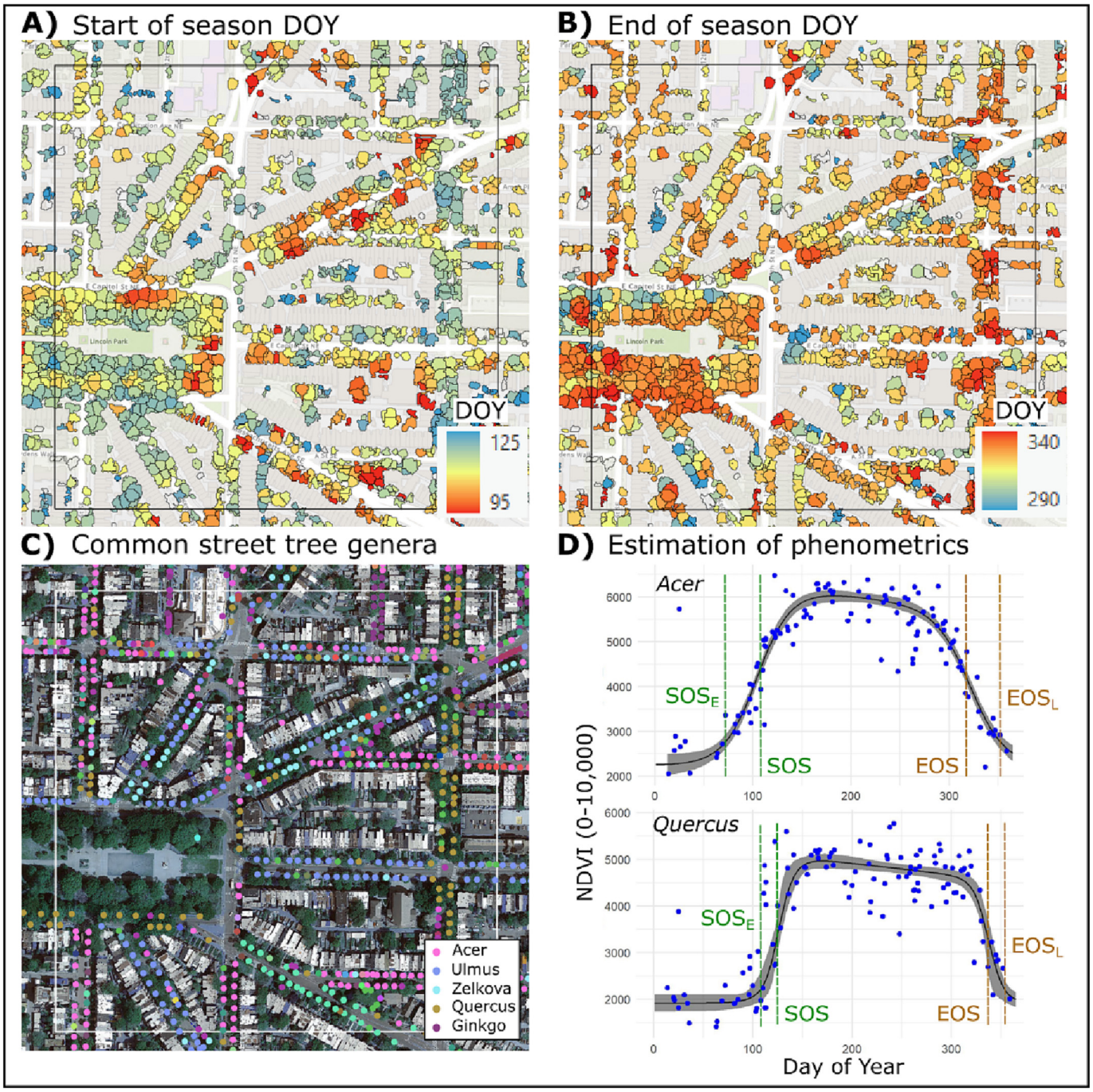

Fig. 2. Examples of crown-scale phenometrics, street tree diversity, and double logistic fits within the Capitol Hill neighborhood of Washington, DC. A) SOS colored by day of year and B) EOS colored by day of year. C) Depiction of street tree diversity in Washington, DC where the legend shows the 5 most common genera. D) Two examples of double logistic fits using aggregated data from 2018 to 2020; vertical dashed lines depict the four phenometrics used in this study and 95 % confidence intervals are shown around the fitted curve. The inner box in A, B, and C is 500 m to provide visual scale.

2.3. Statistical modeling at plot and crown scales

For analysis at 30 m pixel (or "plot") scale, we estimated phenometrics at each plot as a proxy for existing moderate-resolution remote sensing methods. These were mostly mixtures of trees, low vegetation, grass, and/or impervious surfaces. Therefore, we also calculated average phenometrics within each plot for trees alone, grass alone, and low vegetation alone using the crown-scale data. Determination of plant functional types (PFT) within plots, as well as the fractional cover of trees within each plot, came from a canopy height model of the study area derived from lidar; heights <1 m were designated "grass", between 1 and 4 m were designated "shrub", and >4 m were designated "trees". We modeled the influence of standardized PFT and site characteristics on SOS and EOS using ordinary least squares (OLS) regression. Site variables (Table 1) were deemed to exhibit influence if they were in the model with the lowest Bayesian Information Criterion (BIC). We evaluated both PFT and site – in terms of their relative contributions to predicting SOS and EOS – by creating three sets of models for each response variable. These contained 1) only site variables, 2) only PFT variables (grass fractional cover, canopy fractional cover), 3) both site and PFT variables.

To incorporate species information into our analyses, we estimated crown-scale models. Given the near-nadir view, 3 m resolution, and low

Table 1
Response and candidate predictor variables considered for modeling site controls on phenometrics. The "Selected for" column notes which variables were ultimately included in our models based on model selection criteria explained in the text.

Variables	Selected for	Description
Response		
SOS	NA	Start of season (day of year)
EOS	NA	End of season (day of year)
Predictor		
air_temp	EOS	Air temperature from August 2018 field campaign averaged within 90 m radius of tree
elevation	SOS and EOS	Elevation from lidar DTM
imperviousness	SOS and EOS	Impervious surface fraction within 90 m radius of tree from local planimetric data
income		Median household income for DC census tracts
insolation		Modeled solar insolation in summertime, proxy for shade map, used lidar DSM
landform		Concave, convex, or flat topography classes based on lidar DTM
latitude	SOS and EOS	Latitude to mitigate spatial autocorrelation and account for unexplained spatial variation
longitude	SOS and EOS	Longitude to mitigate spatial autocorrelation and account for unexplained spatial variation
patch		Percent cover by a large patch of canopy within 90 m
planting_space		Size of tree box or strip for street trees in square meters
tree_canopy	EOS	Tree canopy fractional cover within 90 m of tree

Table 2
Species included in the study. Initially there were 63,019 street trees and 29 species included in the dataset. After filtering by tree size and other criteria, 10,358 trees and 26 species were retained for use in the PGLS models.

Species botanical name	Count	PGLS count
Acer platanoides	1669	43
Acer rubrum	8389	752
Acer saccharum	2725	222
Celtis occidentalis	830	7
Cercis canadensis	1058	–
Ginkgo biloba	4015	820
Gleditsia triacanthos	788	26
Gymnocladus dioicus	341	–
Lagerstroemia indica	1874	–
Liquidambar styraciflua	1456	124
Liriodendron tulipifera	366	131
Nyssa sylvatica	918	6
Platanus occidentalis	770	236
Platanus × *acerifolia*	3756	77
Prunus serrulata 'Kwanzan'	714	6
Prunus yedoensis	644	9
Quercus acutissima	807	79
Quercus bicolor	1247	13
Quercus coccinea	1589	433
Quercus lyrata	612	22
Quercus palustris	5596	2196
Quercus phellos	5838	2130
Quercus rubra	2955	968
Tilia americana	678	201
Tilia cordata	1827	165
Tilia tomentosa	742	6
Ulmus americana	5170	1375
Ulmus parvifolia	2255	25
Zelkova serrata	3390	286
Total	63,019	10,358

nominal positional uncertainty of PlanetScope data (2.6 m), there was good spatial registration of crowns from one image to the next. However, to minimize noise in this study we chose to only retain large trees with diameter at breast height >50.8 cm (20 in) and height >10 m (Table 2; full data filtering details in Supplementary materials S1). This reduced the sample size from 63,019 to 10,358 crowns. After filtering, we fit two types of models to SOS and EOS: 1) OLS models where fixed effects were site characteristics and 2) phylogenetic generalized least squares (PGLS; Revell, 2010) mixed-effects models where fixed effects were species identity or species identity plus site characteristics and random effects were species or species nested within year. PGLS was used to account for residual correlation due to species relatedness. For both PFT and crown-scale models, models were run 100 times with a subset of observations (n = 750) to minimize spatial autocorrelation of the crown-scale residuals and to generate plausible ranges for model coefficients and fit metrics (e.g., R^2 and median absolute difference). Further details on PGLS and model details such as mitigation of spatial autocorrelation appear in Supplementary materials S2.

Although the core models in this study use data aggregated by year (2018–2020) to focus on the time-independent effects of species and site on phenometrics, we also ran year-specific models. The primary motivations were to: 1) assess the explanatory power of the integrated model compared to one that included year and 2) facilitate further examination of the importance of species in determining the timing of SOS and EOS (i.e., do species alter their phenology in concert from year to year?). Note: All uncertainty in this research is presented as 95 % confidence interval of the statistic in question unless otherwise stated.

3. Results

3.1. Crown-scale analysis improves phenological mapping capabilities

Compared to simulated 30 m pixels, phenometric uncertainty at the crown scale was lower by 14 % for both SOS (from ±5.41 to ± 4.66 days) and EOS (from ±6.82 to ±5.87 days). This reduction in median uncertainty (crown/pixel 95 % confidence interval on the double logistic fit) highlights the improved ability of the high-resolution spatial analysis to isolate tree species and plant functional types. Also, this is likely a conservative estimate of uncertainty reduction because it does not account for the higher temporal resolution of PlanetScope imagery compared to best-available 30 m data (e.g., Harmonized Landsat-Sentinel; Bolton et al., 2020). Moreover, the fine-scale maps (Fig. 2) yielded more usable measurements, particularly in densely built-up areas. Specifically, the phenological curve fitting failure rate due to environmental noise or sensor issues was 30.9 % when aggregating the 3 m Planet data to 30 m pixels but for only 12.6 % when aggregating to the individual crown scale.

Over the last several decades, MODIS has provided the best-available temporal resolution for phenological monitoring (1–2-day revisit interval) but MODIS data have a coarse spatial resolution (250 or 500 m pixel size) and images are commonly composited over 8-day periods (Adole et al., 2019; Ganguly et al., 2010). When comparing our crown-scale dataset with simulated 250 m MODIS pixels (Fig. S2), there was strong agreement between SOS and EOS at the pixel-scale and the averaged crown-scale values contained within, but only for pixels with high tree canopy fractions (Fig. 3); above 50 % cover, the average difference was 1.1 days for SOS and 1.5 days for EOS. However, most locations in urban areas have canopy fractions <50 % and, under these conditions, the difference increased to 2.4 days for SOS and 4.7 days for EOS (Fig. 3). Understanding the magnitude and drivers of phenological variability is thus hindered by large pixels that have low vegetation fractional cover, intermix plant functional types, and contain multiple tree species in heterogeneous assemblages.

3.2. Pixels containing diverse PFT may overstate the advance of SOS

We found that moderate and coarse resolution remote sensing methods can overstate the influence of an urban setting on tree phenology by mixing plant functional types within pixels. In Washington, DC, grass and other vegetation <1 m in height covered 11.9 % of the land area whereas trees covered 34.5 %. Median grass SOS (Fig. S3) was estimated to occur at DOY 95.5 ± 1.9 whereas tree SOS occurred >16 days later at 111.8 ± 0.62 (with shrubs between 1 and 4 m at DOY 109.4 ± 0.76). Urban 30 m pixels commonly contain a mixture of surface materials and/or vegetation,

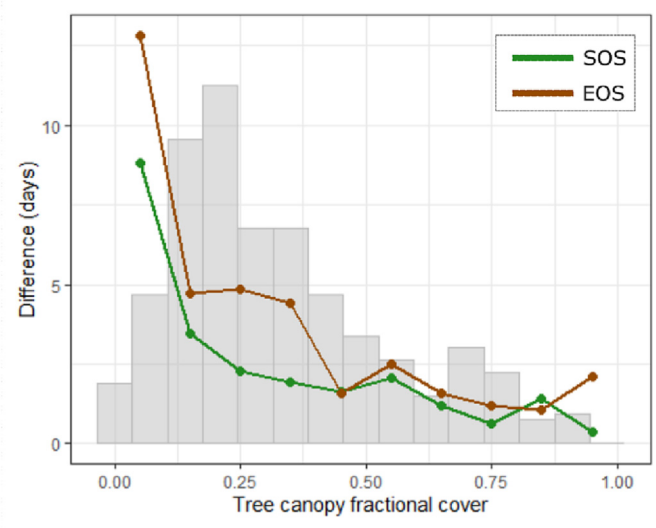

Fig. 3. Difference between MODIS-scale and crown-scale phenology across a gradient in canopy fractional cover. Agreement is depicted as the median absolute difference (in days) between simulated 250 m MODIS pixel-scale and summarized crown-scale estimates of SOS and EOS across ten fractional cover bins. The histogram in the background depicts the distribution of canopy cover across Washington, DC.

possibly including trees, grass, and shrubs in a single pixel. As a result, estimates of "tree" SOS in cities could be 1.8 ± 1.3 days early. In the case of the early measure of start of season (SOS_E; akin to 15 % green-up, Fig. 2D; Moon et al., 2021) the potential deviation increased to 3.5 ± 1.3 days, highlighting the earlier initiation of green-up by grass but also its slower progression. The divergence is smaller for measures of EOS, where grass senesces 9.6 ± 3.1 days earlier than trees, on average, and a mixed-PFT pixel assessment may understate the delay in tree EOS by 0.9 ± 1.8 days. Therefore, it seems plausible that PFT, more than within-city locational context, may exert a strong influence on estimates of urban vegetation phenology.

We modeled SOS and EOS at 30 m resolution (the highest spatial resolution of typical remote sensing time series; equivalent to Landsat) using OLS regression to assess the relative contributions of PFT and site factors (e.g., imperviousness, elevation, air temperature spatial anomaly; Table 1; Table 3). Site factors contributed only minimally to variation in SOS and negligibly to that in EOS. Surrounding tree canopy and impervious surface cover within 90 m explained only 7 % of the variation in crown-scale SOS (Fig. 4A; Table 3). Inclusion of PFT information increased model explanatory power to 18 % with grass cover as the critical addition (see standardized coefficients in Table 3). Contrary to expectations, site conditions (e.g., local imperviousness) had no bearing on the timing of EOS. However, accounting for sub-pixel grass and tree cover raised EOS models' predictive power modestly (R^2 = 0.10; Fig. 4A) and also allowed us to identify the effects of local air temperature and imperviousness, which were not differentiable from zero in the mixed-pixel dataset. The standardized coefficients suggest that, when PFT is known, grass cover relates to earlier pixel-level senescence while sub-pixel tree cover, imperviousness, and temperature anomaly all serve to delay EOS (Table 3). Thus, it is clear that the composition of PFTs in the city is a relevant driver of EOS, but the spatial predictive power of these models is low, potentially highlighting the importance of species variability that is obscured when working with 30 m pixels.

3.3. Species composition governs urban SOS and EOS more than site factors

For large trees that were consistently observable by the PlanetScope satellite constellation, the timing of both SOS and EOS were primarily governed by variation in species identity. We used a phylogenetic mixed model to differentiate the effects of species from each tree's planting site and found that the combination of species and site information explained 51 % and 52 % of variation in SOS and EOS across the study area, respectively (Fig. 4B). The dominant contribution to these models' explanatory power was species identity (the random effect), as evidenced by species-only models explaining 47 % and 42 % of SOS and EOS timing. Contributions of site factors were clearly limited in SOS models (they reduced the median absolute difference or, MAD, from 3.1 to 3.0 days) but, as anticipated, were more relevant for EOS (and reduced MAD from 5.8 to 5.0 days; Fig. 4D). Using a BIC-based variable selection process, the final model included information about local air temperature, imperviousness, tree canopy, and elevation, where temperature was the most important predictor (see standardized coefficients in Table 3 and coefficient confidence intervals in Fig. S4). Specifically, we found that, on average, for every 1 °C of increase in local air temperature, EOS was delayed by 1.3 ± 1.2 days. Further, we found that impervious cover within 90 m of each tree, which we interpret as an aggregate measure of urban density, was associated with a 0.44 ± 0.50-day delay in EOS for each 10 % increase in imperviousness, after accounting for variation in air temperature. Some species were more susceptible to site factors than others, as indicated by model explanatory power (Fig. S5) with median R^2 values ranging from <0.1 (e.g., *Ulmus americana*) to ~0.3 (e.g., *Liquidambar styraciflua*). These

Table 3
Standardized coefficients of ordinary least squares (OLS) and phylogenetic generalized least squares (PGLS) mixed models of SOS or EOS based on site factors, species, or both. Models were constructed at either the "30 m pixel" or "crown" scales through, in both cases, aggregation of 3 m Planet data. All variables except for longitude and latitude were always significantly different from zero at $p < 0.001$ (non-significant values in red). R^2 is the median from all model runs. MAD is the median absolute difference in days (also median from all model runs). Variable explanations appear in Table 1.

	Model		Site factors						Species or PFT			Eval.	
	Model	Type	*imperv.*	*air_temp*	*elev.*	*canopy*	*lon.*	*lat.*	*%tree*	*%grass*	*species*	R^2	MAD
30 m pixel	SOS site	OLS	0.26			0.29	0.08	0.1	NA	NA		0.07	7.2
	SOS PFT	OLS							0.11	-0.34		0.15	7.2
	SOS full	OLS	0.22			0.14	0.07	0.1	0.16	-0.29		0.18	6.8
	EOS site	OLS	0.09				0	-0.01	NA	NA		0.01	11.2
	EOS PFT	OLS							0.12	-0.18		0.06	12.3
	EOS full	OLS	0.15	0.11			0.03	-0.03	0.29	-0.11		0.10	10.7
Crown scale	SOS site	OLS	-0.04		0.21		0.24	-0.02			NA	0.09	3.9
	SOS spp	PGLS									Yes	0.47	3.1
	SOS full	PGLS	-0.07		0.09		0.14	-0.03			Yes	0.51	3.0
	EOS site	OLS	0.05	0.11			0.11	-0.15			NA	0.10	7.7
	EOS spp	PGLS									Yes	0.42	5.8
	EOS full	PGLS	0.06	0.11	-0.04	0.04	0.13	-0.13			Yes	0.52	5.0

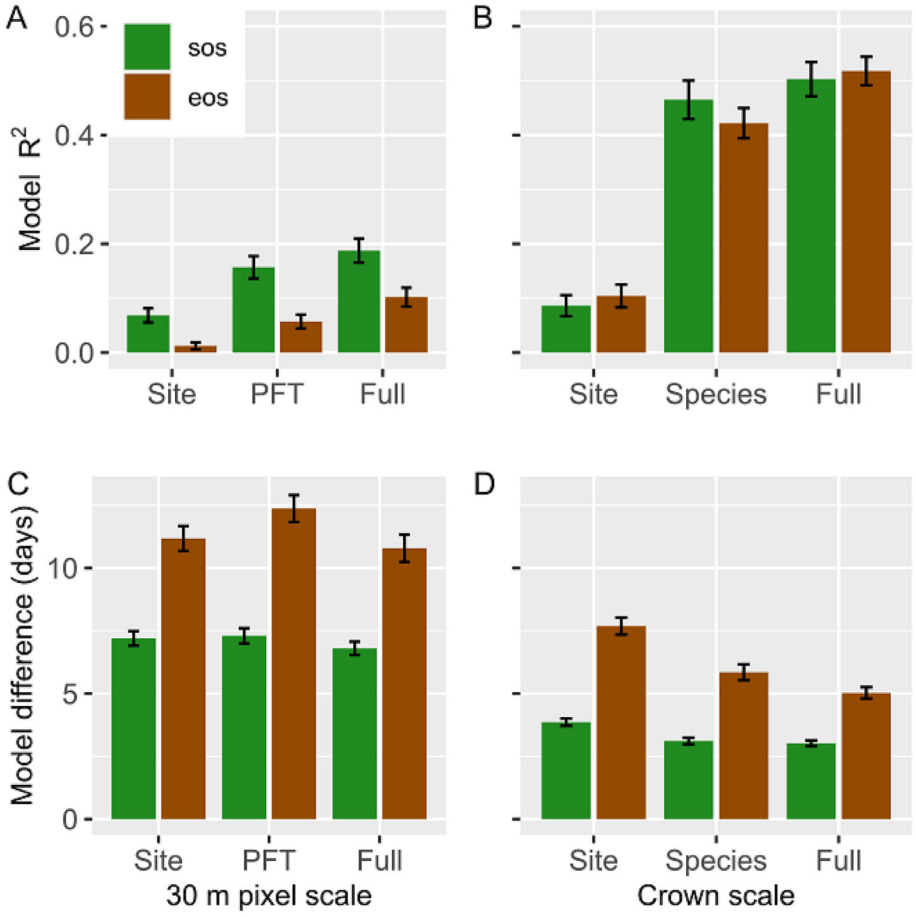

Fig. 4. Model comparisons. (A and B) Model explanatory power (R^2) and (C and D) mean model difference (in days) when modeling SOS and EOS using site factors only (denoted Site), species identity or plant functional type only (denoted PFT or Species, respectively), or combined, mixed models (denoted Full). Error bars are standard deviations of these quantities across 100 model fits on random subsets of the data. In (A and C), phenometrics were derived from pixels aggregated to the resolution of Landsat imagery (30 m); in (B and D), phenometrics come from crown-scale data.

results highlight species sensitivity to conditions with, for example, local temperature potentially playing a strong role in certain species' EOS timing.

3.4. Species rank order of phenological events maintained across years

Spring and summer temperatures and precipitation conditions were distinctly different in 2018, 2019, and 2020 (Fig. 5), providing a means to examine how synchronous or divergent responses to environmental conditions were across species. Maintenance of phenometric rank order

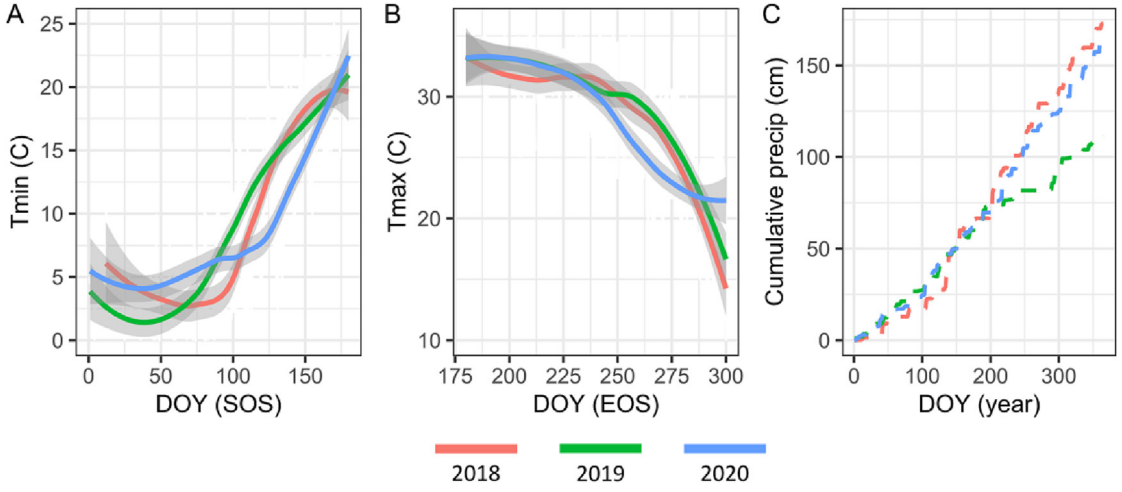

Fig. 5. Weather data for 2018–2020. Temperature (solid) and precipitation (dashed) trends in the study area for each year. A) Daily minimum air temperature values (°C, smoothed) for DOY 1–180; B) daily maximum temperatures for DOY 180–300; C) cumulative precipitation (cm), full year.

(Geng et al., 2020) in this environment could imply lower within-species phenological plasticity driven by site conditions and an elevated importance of urban species composition in governing spatial variability in our phenological response variables. Species rank order was most stable during green-up as evaluated using SOS: Spearman rank correlations were consistently high and internal stability was strong (based on Cronbach's α being ≥0.95; Figs. 6A, 7A). As expected, given the increased influence of site and accumulated stress during the growing season, rank order stability declined somewhat for EOS (Figs. 6B, 7B) but still was generally high. SOS average pairwise rank correlation was 0.89 compared to an EOS value of 0.76, highlighting the comparatively high level of green-up stability. Genera that flushed relatively early, such as *Zelkova*, leafed out progressively earlier each year, aligning with year-by-year increases in average daily minimum March temperatures (Figs. 5A, 7A). In contrast, the late-flushing genus *Platanus* appeared to respond more to late April average daily minimum temperatures wherein 2019 was much warmer than either other year (Figs. 5A, 7A). Although this study focuses primarily on the relative importance of species versus site effects, it is worth noting that the explanatory power of an SOS model incorporating year *and* species as nested random effects was substantially higher than the year-aggregated model (R^2 = 0.70 nested versus R^2 = 0.51 aggregated), owing to the well-established importance of winter and spring conditions on the timing of leaf development. EOS generally tracks late summer temperature trends, most notably with the latest average EOS in 2019 (when temperatures were highest from September onward) and the largest variation in EOS (i.e., greatest interspecific differences in the timing of senescence) corresponding to an early but gradual cooling in 2020 (Figs. 5B, 7B). In models of EOS, accounting for year was less valuable, only negligibly raising the full model R^2.

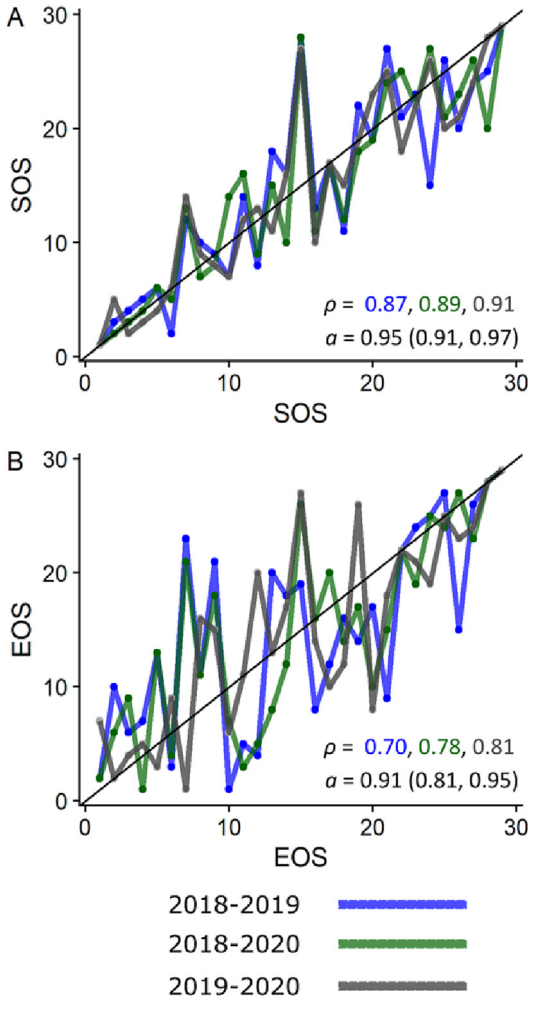

Fig. 6. Rank order stability in phenometrics. Pairwise (by year) species rank order stability for 2018–2019, 2018–2020, and 2019–2020 for A) SOS and B) EOS phenometrics accompanied by Spearman's rank correlation (ρ) and Cronbach's alpha (α) with 95 % confidence intervals.

4. Discussion

We were able to distinguish species and site controls on urban tree phenology by leveraging high-resolution remote sensing workflows and drawing on ground-level data for thousands of trees. Our core finding is that SOS and EOS, when derived from satellite remote sensing data, primarily vary with species composition or PFT rather than environmental characteristics of the planting location. This implies that, in cities, tree phenological change in response to changing temperature regimes may be smaller than has been estimated using moderate-resolution phenological observations. Still, tree location did influence the timing of EOS; local air temperature, impervious surface cover, surrounding tree canopy, and elevation all exhibited significant effects on EOS. It is important to note that this study examined fine-scale, *within-city* variation in site factors and did not span the full urban-rural gradient. Nonetheless, our urban setting provided a data-rich laboratory for addressing questions of phenological plasticity in biodiverse environments, likely applying well beyond cities. Moreover, our dataset and workflow may be a launching point for projects seeking to characterize and map invasive species distributions (especially of understory plants), the health status of urban trees, and urban ecosystem productivity (Fang et al., 2020; Granero-Belinchon et al., 2020; Singh et al., 2018).

4.1. High spatial and temporal resolution, satellite-based phenological analysis

Investigations of land surface phenology using cameras or other sensors are now common, but there are trade-offs among spatial resolution, spatial extent, and frequency of observations. Ground-based phenocam networks provide sub-daily imagery across a wide range of ecosystems, albeit with overrepresentation of North America and Europe (Richardson et al., 2018). Satellite-based studies allow for continental and global scale estimation at near-daily temporal resolution (Adole et al., 2019; Bolton et al., 2020; Ganguly et al., 2010) but usually at 500 m pixel size. In our study, in areas of high vegetation cover, there was strong agreement (R^2 = 0.94) between our estimates of SOS and EOS and those derived from Multi-Source Land Surface Phenology (MS-LSP) data which is estimated from harmonized Landsat-Sentinel imagery (HLS; Fig. S1; Moon et al., 2021). However, 3-m pixel data from PlanetScope can resolve features ~1/100th the size of those observable with HLS datasets and with scenes nominally available daily at mid-latitudes, instead of ~3 days (Bolton et al., 2020; Moon et al., 2021, 2022). This allows for the retrieval of phenometrics from individual trees even in densely built-up urban environments, representing areas previously avoided due to low vegetation cover (Melaas et al., 2016; Zhang et al., 2004). With the methods established in this study and similar datasets recently released by Moon et al. (2022), there is a path towards a more process-based understanding underpinning regional scale carbon, water, and energy fluxes; efforts previously hampered by imprecise or spatially constrained land surface phenology datasets. A dataset of this resolution also offers increased viability, in heterogeneous landscapes, for upscaling approaches from plot-based landscape phenology to coarse resolution land surface phenology from satellite (Liang et al., 2011).

4.2. Mixing of PFTs at sub-pixel scale can cause overestimates of SOS advance

Although there is an apparent relationship between urban density and an extended growing season at moderate to coarse spatial scales (Li et al., 2019; Li et al., 2017a; Li et al., 2017b; Meng et al., 2020; Zhang et al., 2004), our results suggest that this relationship is, at least in part, an artifact of sub-pixel PFT mixtures. In measurements focusing on SOS_E, the effect was most pronounced, with mixed 30 m pixels showing green-up timing 3.5 days earlier than tree-only pixels. Our results highlight potential

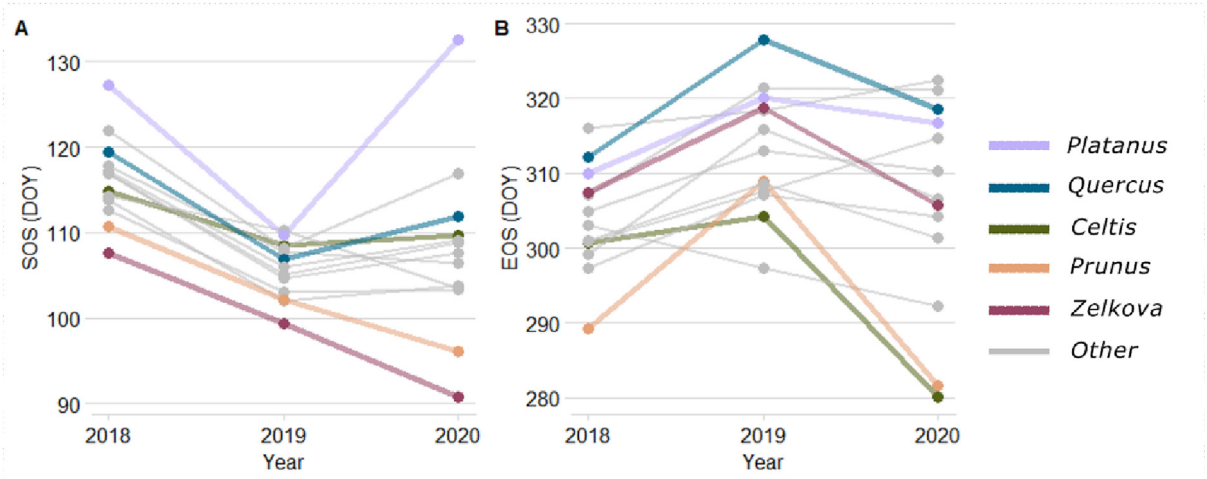

Fig. 7. Interannual variation in phenological responses by genus. Median day of year of A) SOS and B) EOS for genera in 2018, 2019, and 2020.

contributions of phenologically unique understory vegetation such as turfgrass or shrubs in the overall signal (Shustack et al., 2009; Singh et al., 2018). For SOS, the difference of 1.8 days is still substantial in light of the current magnitude of detected urban-rural differences in GSL from deciduous and mixed forest landscapes of 2 to 2.8 days (Li et al., 2017a). At coarse resolution, there is also substantial noise in the annual phenological signal in densely built urban zones (i.e., locations with greater PFT mixtures and more impervious surface), increasing the uncertainty of phenometric estimates (Li et al., 2017b). We found that, at a 250 m pixel size, the quality of relationship between MODIS-scale and crown-scale estimates of phenometrics was largely a function of tree fractional cover within that pixel (Fig. 3). Along an urban to rural gradient, land cover (and particularly the dominance of turfgrass in suburban developments) has been found to strongly control the observed timing of start and end of season phenometrics (Zipper et al., 2016). Beyond the city as well, phenological shifts may be driven by PFT compositional shifts such as understory shrub invasion or, plausibly, overstory vine proliferation (Fridley, 2012; Polgar et al., 2014). Given the recent widespread availability of lidar data in urban and peri-urban environments, a straightforward improvement in remotely sensed phenological inquiry could be to partition the landscape by height class as a proxy for PFT. Still, PFT delineation does not fully account for either species' genetic differences or preferential planting legacies that continue to undercut the precision of landscape-scale phenological inquiry (Buyantuyev and Wu, 2012).

4.3. Species composition and spring weather variability control the timing of SOS

Species effects largely governed the SOS signal in this biodiverse study area, highlighting the strong linkage between genetic and functional diversity and the necessity of higher resolution data to study species-level variation (Cleland et al., 2007). During spring green-up, models of SOS were accurate at the crown scale regardless of whether site factors were included (MAD = 3.0 days full model; MAD = 3.1 days for species only; Fig. 4B). This is consistent with evidence from imaging spectroscopy demonstrating that intra-specific variability in functional trait diversity is lower than inter-specific variation, even along strong environmental gradients (Asner et al., 2014). This may be due to limited intra-species phenological plasticity across temperature or photoperiod gradients (Tang et al., 2016).

When disaggregated by year, the primary driver of SOS timing was correlated with interannual variation, as judged by large increase in explanatory power when species was nested within year in a hierarchical model. Depending on seasonal patterns, species phenological synchronicity can be high (e.g., anomalously warm late winter) or low (e.g., protracted cool spring), promoting larger interspecific differences (Geng et al., 2020). In 2019, a rapid increase in spring temperatures drove synchronous green-up of all individuals thus limiting the manifestation of a site-based phenological gradient. By contrast, in 2020, temperatures were stable from February through April, facilitating divergent green-up among species and along a gradient of imperviousness (Fig. 7A). With high synchronicity, site factors (e.g., urban heat island) have limited impact on phenometrics but when synchronicity is low, site factors can explain a higher proportion of phenological variability (Zipper et al., 2016). While green-up timing and synchronicity changed from year-to-year, species rank order was largely unchanged reflecting coincident response based on genetic similarity (Fig. 6A). For example, our data show that early flushing, non-native genera such as *Zelkova* and *Prunus* and later flushing *Platanus* were pushed to even earlier or later SOS timings respectively when late winter was warm but mid-spring was cool (Fig. 7A). This is consistent with findings elsewhere that early budburst species with warmer initial ranges tend to advance start of season more rapidly in response to warming (Gunderson et al., 2012). A dataset such as in this study applied to other landscapes could help to clarify drivers of species phenological plasticity through large-N observational monitoring. There remains uncertainty surrounding the extent to which, for example, early flushing species will continue to green-up earlier under warming or whether this shift will be limited to minimize freeze risk or by intrinsic photoperiod constraints (Geng et al., 2020; Rollinson and Kaye, 2012; Tang et al., 2016).

4.4. Species and site factors contribute the timing of urban tree EOS

The timing and drivers of EOS for trees is less certain than for SOS in both urban and natural environments (Jochner and Menzel, 2015; Zhang et al., 2004). In the urban environment there is time for local environmental stressors to accumulate and enhance variability in EOS timing. Alternatively, the atmospheric urban heat island effect may be minimized in late summer and early fall time periods, thus muting variability along the urban-rural gradient (Jochner and Menzel, 2015). We found EOS timing also to be largely controlled by species albeit with more contribution from site fixed effects compared to SOS models (Fig. 4). Although full EOS model explanatory power (R^2 = 0.52) was similar to that of the SOS model (R^2 = 0.50), the reduction in explanatory power when only considering species is more pronounced (species only R^2 = 0.42 for EOS; Fig. 4A). Local air temperature within a 90 m buffer was the key driver of within-species delay in EOS (Table 3). Although temperature-driven delay in EOS is consistent with current literature employing either land surface temperature or imperviousness as urban heat proxies (Chi et al., 2022; Li et al., 2019; Zhang et al., 2004), the relationship may reverse under extreme heat, water limitation, or high vapor pressure deficit conditions, resulting in a form of “accelerated leaf senescence” (Bertold et al., 2019). Here, we observed almost all species with a positive relationship between temperature

and EOS, with several exceptions (Fig. S5). However, for species exhibiting an earlier EOS with warmer air temperatures, the ability to model EOS was generally quite low, potentially because they are small or otherwise difficult to observe from satellite (e.g., *Celtis occidentalis*). There is thus a need for additional inquiry into species that may respond differently to warming. Similarly, more detailed study of local site conditions is needed across urban morphologies and regions (Li et al., 2022). While we found a significant influence of air temperature and imperviousness, many other spatial predictors (e.g., insolation, landform, planting space characteristics; Table 1) did not meet thresholds for model inclusion, and still other potentially important variables (e.g., soil conditions, nighttime lights) remained out of scope (Wohlfahrt et al., 2020).

4.5. Limitations and summary

This high-resolution workflow allows for previously impractical analyses that are simultaneously fine-scale and at large spatial extents. However, there are limitations that point to opportunities for future work. Although we had access to >60,000 street trees, this data source also represents a limitation since it only represents street trees and it is constrained to the urban environment (i.e., does not represent a full urban to rural gradient.) Both factors constrain the range of planting site variables (e.g., *air temperature*, *imperviousness*). Future studies might add a ground data collection component (e.g., single species transects along the gradient of urban built density) or incorporate tree inventories from multiple, adjoining municipalities. It is also challenging to fully characterize planting site characteristics. Previous research makes it clear that temperature and imperviousness can be important, but it is additionally likely that variables relating to soil properties and site-specific moisture regimes would also play a role in tree phenology. Concerning remote sensing data, future studies will benefit from improved radiometry of commercial satellite data. Consistent with Moon et al. (2022), we found that that PlanetScope red-band reflectance did not correspond well for all years with co-located HLS red values (though NIR alignment was good). This was notable in 2020 and thus added uncertainty to, particularly, our EOS 2020 phenometric values. More recently launched instruments (e.g., PS2.SD, PSB.SD) employ newer technologies that will likely yield improvements in radiometric precision and accuracy.

In summary, this paper highlights the importance of high-resolution data for resolving phenological patterns in urban as well as other heterogeneous environments (J. Wang et al., 2020; Zhao et al., 2022). We found that despite high temporal resolution offered by coarser platforms, inability to isolate PFTs in mixed pixels can lead to phenometric bias that can be exacerbated in dense urban (i.e., low cover but biodiverse) landscapes. Increasing spatial resolution while maintaining temporal frequency allowed us to disentangle the relative importance of species and canopy composition versus site factors in driving spatial variability in both SOS and EOS. Thus, we conclude that part of the apparent lengthening of the urban tree growing season could be attributable to differing planting preferences in urban core versus suburban or rural landscapes as well as fine-scale mixtures of plant functional types. Our workflow provides a template for a wide range of new applications to better understand the role of warming climate on urban, agricultural, and heterogeneous natural ecosystem dynamics.

CRediT authorship contribution statement

Michael Alonzo: Conceptualization, Methodology, Investigation, Visualization, Supervision, Writing – original draft, Writing – review & editing. **Matthew E. Baker:** Conceptualization, Methodology, Writing – review & editing. **Joshua S. Caplan:** Conceptualization, Methodology, Investigation, Writing – review & editing. **Avery Williams:** Investigation, Visualization, Writing – review & editing. **Andrew J. Elmore:** Methodology, Writing – review & editing.

Data availability

Data will be made available on request.

Declaration of competing interest

Authors declare that they have no competing interests.

Acknowledgments

This study was supported by funding from the National Science Foundation (grant no. 1951647) to MA, MEB, and JSC as well as by a Garden Club of America Zone VI Fellowship in Urban Forestry to AW.

Appendix A. Supplementary data

Supplementary data to this article can be found online at https://doi.org/10.1016/j.scitotenv.2023.163818.

References

Achanta, R., Shaji, A., Smith, K., Lucchi, A., Fua, P., Süsstrunk, S., 2012. SLIC superpixels compared to state-of-the-art superpixel methods. IEEE Trans. Pattern Anal. Mach. Intell. 34 (11), 2274–2281. https://doi.org/10.1109/TPAMI.2012.120.

Adole, T., Dash, J., Rodriguez-Galiano, V., Atkinson, P.M., 2019. Photoperiod controls vegetation phenology across Africa. Commun.Biol. 2 (1). https://doi.org/10.1038/s42003-019-0636-7.

Alonzo, M., Baker, M.E., Gao, Y., Shandas, V., 2021. Spatial configuration and time of day impact the magnitude of urban tree canopy cooling. Environ. Res. Lett. 16 (8), 084028. https://doi.org/10.1088/1748-9326/ac12f2.

Alonzo, M., Bookhagen, B., Roberts, D.A., 2014. Urban tree species mapping using hyperspectral and lidar data fusion. Remote Sens. Environ. 148, 70–83. https://doi.org/10.1016/j.rse.2014.03.018.

Asner, G.P., Martin, R.E., Tupayachi, R., Anderson, C.B., Sinca, F., Carranza-Jiménez, L., Martinez, P., 2014. Amazonian functional diversity from forest canopy chemical assembly. Proc. Natl. Acad. Sci. U. S. A. 111 (15), 5604–5609. https://doi.org/10.1073/pnas.1401181111.

Beck, H.E., Zimmermann, N.E., McVicar, T.R., Vergopolan, N., Berg, A., Wood, E.F., 2018. Present and future Köppen-Geiger climate classification maps at 1-km resolution. Sci. Data 5, 1–12. https://doi.org/10.1038/sdata.2018.214.

Bertold, M., Balzarolo, M., Dox, I., Leys, S., Marchand, L.J., Geron, C., Portillo-Estrada, M., AbdElgawad, H., Asard, H., Campioli, M., 2019. Detecting the onset of autumn leaf senescence in deciduous forest trees of the temperate zone. New Phytol., 0–3 https://doi.org/10.1111/nph.15991.

Bolton, D.K., Gray, J.M., Melaas, E.K., Moon, M., Eklundh, L., Friedl, M.A., 2020. Continental-scale land surface phenology from harmonized Landsat 8 and Sentinel-2 imagery. Remote Sens. Environ. 240 (November 2019), 111685. https://doi.org/10.1016/j.rse.2020.111685.

Buyantuyev, A., Wu, J., 2012. Urbanization diversifies land surface phenology in arid environments: interactions among vegetation, climatic variation, and land use pattern in the Phoenix metropolitan region, USA. Landsc. Urban Plan. 105 (1–2), 149–159. https://doi.org/10.1016/j.landurbplan.2011.12.013.

Cadenasso, M.L., Pickett, S.T.a., Schwarz, K., 2007. Spatial heterogeneity in urban ecosystems: reconceptualizing land cover and a framework for classification. Front. Ecol. Environ. 5 (2), 80–88. https://doi.org/10.1890/1540-9295(2007)5[80:SHIUER]2.0.CO;2.

Cheng, Y., Vrieling, A., Fava, F., Meroni, M., Marshall, M., Gachoki, S., 2020. Phenology of short vegetation cycles in a Kenyan rangeland from PlanetScope and Sentinel-2. Remote Sens. Environ. 248 (July), 112004. https://doi.org/10.1016/j.rse.2020.112004.

Chi, D., Van Meerbeek, K., Yu, K., Degerickx, J., Somers, B., 2022. Foliar optical traits capture physiological and phenological leaf plasticity in Tilia × euchlora in the urban environment. Sci. Total Environ. 805, 150219. https://doi.org/10.1016/j.scitotenv.2021.150219.

Cleland, E.E., Chuine, I., Menzel, A., Mooney, H.A., Schwartz, M.D., 2007. Shifting plant phenology in response to global change. TrendsEcol.Evol. 22 (7), 357–365. https://doi.org/10.1016/j.tree.2007.04.003.

Elmore, A.J., Guinn, S.M., Minsley, B.J., Richardson, A.D., 2012. Landscape controls on the timing of spring, autumn, and growing season length in mid-Atlantic forests. Glob. Chang. Biol. 18 (2), 656–674. https://doi.org/10.1111/j.1365-2486.2011.02521.x.

Fang, F., McNeil, B.E., Warner, T.A., Maxwell, A.E., Dahle, G.A., Eutsler, E., Li, J., 2020. Discriminating tree species at different taxonomic levels using multi-temporal WorldView-3 imagery in Washington D.C., USA. Remote Sens. Environ. 246 (March), 111811. https://doi.org/10.1016/j.rse.2020.111811.

Fridley, J.D., 2012. Extended leaf phenology and the autumn niche in deciduous forest invasions. Nature 485 (7398), 359–362. https://doi.org/10.1038/nature11056.

Ganguly, S., Friedl, M.A., Tan, B., Zhang, X., Verma, M., 2010. Land surface phenology from MODIS: characterization of the Collection 5 global land cover dynamics product. Remote Sens. Environ. 114 (8), 1805–1816. https://doi.org/10.1016/j.rse.2010.04.005.

Geng, X., Fu, Y.H., Hao, F., Zhou, X., Zhang, X., Yin, G., Vitasse, Y., Piao, S., Niu, K., De Boeck, H.J., Menzel, A., Peñuelas, J., 2020. Climate warming increases spring phenological

differences among temperate trees. Glob. Chang. Biol. 26 (10), 5979–5987. https://doi.org/10.1111/gcb.15301.
Granero-Belinchon, C., Adeline, K., Lemonsu, A., Briottet, X., 2020. Phenological dynamics characterization of alignment trees with sentinel-2 imagery: a vegetation indices time series reconstruction methodology adapted to urban areas. Remote Sens. 12 (4). https://doi.org/10.3390/rs12040639.
Gunderson, C.A., Edwards, N.T., Walker, A.V., O'Hara, K.H., Campion, C.M., Hanson, P.J., 2012. Forest phenology and a warmer climate – growing season extension in relation to climatic provenance. Glob. Chang. Biol. 18 (6), 2008–2025. https://doi.org/10.1111/j.1365-2486.2011.02632.x.
Jenerette, G.D., Clarke, L.W., Avolio, M.L., Pataki, D.E., Gillespie, T.W., Pincetl, S., Nowak, D.J., Hutyra, L.R., McHale, M., McFadden, J.P., Alonzo, M., 2016. Climate tolerances and trait choices shape continental patterns of urban tree biodiversity. Glob. Ecol. Biogeogr. 25 (11). https://doi.org/10.1111/geb.12499.
Jochner, S., Menzel, A., 2015. Urban phenological studies—past, present, future. Environ. Pollut. 203, 250–261. https://doi.org/10.1016/j.envpol.2015.01.003.
Li, D., Stucky, B.J., Baiser, B., Guralnick, R., 2022. Urbanization delays plant leaf senescence and extends growing season length in cold but not in warm areas of the Northern Hemisphere. Glob. Ecol. Biogeogr. 31 (2), 308–320. https://doi.org/10.1111/geb.13429.
Li, D., Stucky, B.J., Deck, J., Baiser, B., Guralnick, R.P., 2019. The effect of urbanization on plant phenology depends on regional temperature. Nat.Ecol.Evol. 3 (12), 1661–1667. https://doi.org/10.1038/s41559-019-1004-1.
Li, X., Zhou, Y., Asrar, G.R., Mao, J., Li, X., Li, W., 2017. Response of vegetation phenology to urbanization in the conterminous United States. Glob. Chang. Biol. 23 (7), 2818–2830. https://doi.org/10.1111/gcb.13562.
Li, X., Zhou, Y., Asrar, G.R., Meng, L., 2017. Characterizing spatiotemporal dynamics in phenology of urban ecosystems based on Landsat data. Sci. Total Environ. 605–606, 721–734. https://doi.org/10.1016/j.scitotenv.2017.06.245.
Liang, L., Schwartz, M.D., Fei, S., 2011. Validating satellite phenology through intensive ground observation and landscape scaling in a mixed seasonal forest. Remote Sens. Environ. 115 (1), 143–157. https://doi.org/10.1016/j.rse.2010.08.013.
Lu, X., Keenan, T.F., 2022. No evidence for a negative effect of growing season photosynthesis on leaf senescence timing. Glob. Chang. Biol. 28 (9), 3083–3093. https://doi.org/10.1111/gcb.16104.
Melaas, E.K., Wang, J.A., Miller, D.L., Friedl, M.A., 2016. Interactions between urban vegetation and surface urban heat islands: a case study in the Boston metropolitan region Interactions between urban vegetation and surface urban heat islands: a case study in the Boston metropolitan region.
Meng, L., Mao, J., Zhou, Y., Richardson, A.D., Lee, X., Thornton, P.E., Ricciuto, D.M., Li, X., Dai, Y., Shi, X., Jia, G., 2020. Urban warming advances spring phenology but reduces the response of phenology to temperature in the conterminous United States. Proc. Natl. Acad. Sci. U. S. A. 117 (8), 4228–4233. https://doi.org/10.1073/pnas.1911117117.
Moon, M., Richardson, A.D., Friedl, M.A., 2021. Multiscale assessment of land surface phenology from harmonized Landsat 8 and Sentinel-2, PlanetScope, and PhenoCam imagery. Remote Sens. Environ. 266 (December 2020), 112716. https://doi.org/10.1016/j.rse.2021.112716.
Moon, M., Richardson, A.D., Milliman, T., Friedl, M.A., 2022. A high spatial resolution land surface phenology dataset for AmeriFlux and NEON sites. Sci.Data 9 (1), 1. https://doi.org/10.1038/s41597-022-01570-5.
Núñez-Florez, R., Pérez-Gómez, U., Fernández-Méndez, F., 2019. Functional diversity criteria for selecting urban trees. Urban For.Urban Green. 38 (May 2018), 251–266. https://doi.org/10.1016/j.ufug.2019.01.005.
Oke, T., 1982. The energetic basis of the urban heat island. Q. J. R. Meteorol. Soc. 108 (455), 1–24.
Penuelas, J., Rutishauser, T., Filella, I., 2010. Phenology feedbacks on. Science 324 (May 2009), 887–888.
Planet, 2021. Satellite Imagery and Archive. https://planet.com/products/planet-imagery/.
Polgar, C., Gallinat, A., Primack, R.B., 2014. Drivers of leaf-out phenology and their implications for species invasions: insights from Thoreau's Concord. New Phytol. 202 (1), 106–115. https://doi.org/10.1111/nph.12647.
Revell, L.J., 2010. Phylogenetic signal and linear regression on species data. Methods Ecol. Evol. 1 (4), 319–329. https://doi.org/10.1111/j.2041-210X.2010.00044.x.
Richardson, A.D., Hufkens, K., Milliman, T., Aubrecht, D.M., Chen, M., Gray, J.M., Johnston, M.R., Keenan, T.F., Klosterman, S.T., Kosmala, M., Melaas, E.K., Friedl, M.A., Frolking, S., 2018. Tracking vegetation phenology across diverse North American biomes using PhenoCam imagery. Sci.Data 5, 1–24. https://doi.org/10.1038/sdata.2018.28.
Rollinson, C.R., Kaye, M.W., 2012. Experimental warming alters spring phenology of certain plant functional groups in an early successional forest community. Glob. Chang. Biol. 18 (3), 1108–1116. https://doi.org/10.1111/j.1365-2486.2011.02612.x.
Schott, J.R., Salvaggio, C., Volchok, W.J., 1988. Radiometric scene normalization using pseudoinvariant features. Remote Sens. Environ. 26 (1), 1–16. https://doi.org/10.1016/0034-4257(88)90116-2.
Shandas, V., Voelkel, J., Williams, J., Hoffman, J., 2019. Integrating satellite and ground measurements for predicting locations of extreme urban heat. Climate 7 (1), 5. https://doi.org/10.3390/cli7010005.
Shustack, D.P., Rodewald, A.D., Waite, T.A., 2009. Springtime in the city: exotic shrubs promote earlier greenup in urban forests. Biol. Invasions 11 (6), 1357–1371. https://doi.org/10.1007/s10530-008-9343-x.
Singh, K.K., Chen, Y.H., Smart, L., Gray, J., Meentemeyer, R.K., 2018. Intra-annual phenology for detecting understory plant invasion in urban forests. ISPRS J. Photogramm. Remote Sens. 142 (May), 151–161. https://doi.org/10.1016/j.isprsjprs.2018.05.023.
Swan, C.M., Johnson, A., Nowak, D.J., 2017. Differential organization of taxonomic and functional diversity in an urban woody plant metacommunity. Appl. Veg. Sci. 20 (1), 7–17. https://doi.org/10.1111/avsc.12266.
Tang, J., Körner, C., Muraoka, H., Piao, S., Shen, M., Thackeray, S.J., Yang, X., 2016. Emerging opportunities and challenges in phenology: a review. Ecosphere 7 (8), 1–17. https://doi.org/10.1002/ecs2.1436.
Tucker, C.J., 1979. Red and photographic infrared linear combinations for monitoring vegetation. Remote Sens. Environ. 8, 127–150.
Visser, M.E., Van Noordwijk, A.J., Tinbergen, J.M., Lessells, C.M., 1998. Warmer springs lead to mistimed reproduction in great tits (Parus major). Proc. R. Soc. B Biol. Sci. 265 (1408), 1867–1870. https://doi.org/10.1098/rspb.1998.0514.
Wang, J., Yang, D., Detto, M., Nelson, B.W., Chen, M., Guan, K., Wu, S., Yan, Z., Wu, J., 2020. Multi-scale integration of satellite remote sensing improves characterization of dry-season green-up in an Amazon tropical evergreen forest. Remote Sens. Environ. 246, 111865. https://doi.org/10.1016/j.rse.2020.111865.
Wang, S., Ju, W., Penuelas, J., Cescatti, A., Zhou, Y., Yongshuo, Fu., Huete, A.R., Liu, M., Zhang, Y., 2019. Urban – rural gradients reveal joint control of elevated CO2 and temperature on extended photosynthetic seasons. Nat.Ecol.Evol. 3, 1076–1085.
Wohlfahrt, G., Tomelleri, E., Hammerle, A., 2020. The urban imprint on plant phenology. Nat. Ecol.Evol. 2019 (12), 1668–1674. https://doi.org/10.1038/s41559-019-1017-9.The.
Zhang, B., Brack, C.L., 2021. Urban forest responses to climate change: a case study in Canberra. Urban For.Urban Green. 57 (September 2020), 126910. https://doi.org/10.1016/j.ufug.2020.126910.
Zhang, X., Friedl, M.A., Schaaf, C., Strahler, A., Schneider, A., 2004. The footprint of urban climates on vegetation phenology. Geophys. Res. Lett. 31 (12), 10–13. https://doi.org/10.1029/2004GL020137.
Zhao, Y., Lee, C.K.F., Wang, Z., Wang, J., Gu, Y., Xie, J., Law, Y.K., Song, G., Bonebrake, T.C., Yang, X., Nelson, B.W., Wu, J., 2022. Evaluating fine-scale phenology from PlanetScope satellites with ground observations across temperate forests in eastern North America. Remote Sens. Environ. 283, 113310. https://doi.org/10.1016/j.rse.2022.113310.
Zhu, Z., Zhou, Y., Seto, K.C., Stokes, E.C., Deng, C., Pickett, S.T.A., Taubenböck, H., 2019. Understanding an urbanizing planet: strategic directions for remote sensing. Remote Sens. Environ. 228 (April), 164–182. https://doi.org/10.1016/j.rse.2019.04.020.
Zipper, S.C., Jason, S., Aditya, S., Christopher, J.K., Philip, A.T., Steven II, P.L., 2016. Urban heat island impacts on plant phenology: intra-urban variability and response to land cover. Environ. Res. Lett. 11 (5), 54023.
Ziter, C.D., Pedersen, E.J., Kucharik, C.J., Turner, M.G., 2019. Scale-dependent interactions between tree canopy cover and impervious surfaces reduce daytime urban heat during summer. Proc. Natl. Acad. Sci. U. S. A. 116 (15), 7575–7580. https://doi.org/10.1073/pnas.1817561116.